Population imaging at subcellular resolution supports specific and local inhibition by granule cells in the olfactory bulb

SCIENTIFIC REPORTS

OPEN

Population imaging at subcellular resolution supports specific and local inhibition by granule cells in the olfactory bulb

Received: 13 April 2016
Accepted: 09 June 2016
Published: 08 July 2016

Martin Wienisch & Venkatesh N. Murthy

Information processing in early sensory regions is modulated by a diverse range of inhibitory interneurons. We sought to elucidate the role of olfactory bulb interneurons called granule cells (GCs) in odor processing by imaging the activity of hundreds of these cells simultaneously in mice. Odor responses in GCs were temporally diverse and spatially disperse, with some degree of non-random, modular organization. The overall sparseness of activation of GCs was highly correlated with the extent of glomerular activation by odor stimuli. Increasing concentrations of single odorants led to proportionately larger population activity, but some individual GCs had non-monotonic relations to concentration due to local inhibitory interactions. Individual dendritic segments could sometimes respond independently to odors, revealing their capacity for compartmentalized signaling *in vivo*. Collectively, the response properties of GCs point to their role in specific and local processing, rather than global operations such as response normalization proposed for other interneurons.

The first sensory stages of the brain are thought to format relevant environmental information in an efficient manner that facilitates easy and flexible extraction by downstream areas[1–3]. The olfactory bulb is the first synaptic station for odor information, where inputs from olfactory sensory axons are processed by a complex network of neurons before they are conveyed to higher brain areas through mitral/tufted (M/T) cells[1,3–7]. Interneurons in the glomerular layer may play a role in gating inputs to the olfactory bulb[7–10], normalizing the inputs based on the overall level of input[9,11] and temporal patterning of principal neuron activity[12,13]. A gain normalizing role has also been assigned to a sparse population of parvalbumin-positive interneurons in the external plexiform layer[14,15].

Local bulbar processing in the deeper layers of the OB is thought to involve axon-less interneurons called granule cells (GCs), which are ~10 times more numerous than M/T cells[16]. They receive synaptic inputs from M/T cells on their apical dendrites, and make reciprocal inhibitory synapses on M/T cell dendrites. These synapses mediate auto- as well as lateral inhibition across populations of M/T cells[16,17]. The spatial extent and rules governing the connectivity between M/T cells and GCs are not well understood. In addition, since GCs can release transmitter even in the absence of action potentials[18–20], they are capable of local dendritic processing in addition to cell-wide activation[17,21–23]. The extent to which such local processing, which could have important consequences for the computational capabilities of the OB[21,24,25], occurs *in vivo* remains unknown. In addition to feed-forward sensory inputs, GCs also receive extensive feedback from olfactory cortical areas[26–29].

GCs are thought to play a role in temporal patterning of activity in M/T cells[13,25,30–35], and context dependent lateral interactions within the OB[9,31,34]. At a behavioral level, the extent of their activation can influence odor discrimination times[36,37]. Theoretical and computational studies have also suggested a role for GCs in pattern separation and decorrelation[24,38]. There is, however, some uncertainty about the extent of GC influence on some aspects of MC activity[13]. In this regard, cortical feedback is thought to flexibly alter the activity of GCs based on experience and context[26,28,39–41]. GC activity *in vivo* has been recorded using electrophysiological techniques, but the relatively low yield of this technique has prevented a comprehensive view of the repertoire of GC responses to odors[42–46]. Recent experiments using multiphoton imaging of populations of GCs have revealed interesting features of GC activity, for example that they are weakly and sparsely activated in anesthetized mice, and become more densely activated in awake mice[39], a finding confirmed by electrophysiological recordings[46].

Center for Brain Science and Department of Molecular & Cellular Biology Harvard University, Cambridge 02138, MA, USA. Correspondence and requests for materials should be addressed to V.N.M. (email: vnmurthy@fas.harvard.edu)

Despite the welcome resurgence of research on GC function, none of these studies have shed light on how GC activity relates to the statistics of inputs to the OB (glomerular activation patterns, for example), nor have they examined the subcellular local activation of GCs *in vivo*. More generally, many key questions about the spatio-temporal dynamics of activity in GCs and their relation to sensory stimuli remain to be addressed. Here, we have used multiphoton microscopy and calcium imaging to examine odor responses in a large population of GCs, both in their somata as well as in their dendrites.

Results

We used viral expression of GCaMP3[47] to investigate odor-evoked activity in GCs of adult mice. In a few experiments that are flagged clearly, we also used a more sensitive indicator GCaMP5. To assist in identification of infected cells, we also co-expressed dTomato in these cells using the 2A viral element (Supplementary Fig. S1). We injected AAV2/9 virus into one or both olfactory bulbs, and waited for 3 weeks or more before imaging. Infected OBs were visualized after removal of the overlying bone with wide-field fluorescence imaging (Supplementary Supplementary Fig. S1). Immunohistochemical analysis revealed that GCs can be readily labeled with dTomato and GCaMP3, with negligible infection in mitral cells, at least with AAV2/9 at the titers used in this study (Fig. 1A, Supplementary Fig. S1). Even if a few mitral cells were labeled, GCs could be readily identified by their smaller size and deeper locations.

We used multiphoton microscopy to image GC somata and apical dendrites in anesthetized mice. In the external plexiform layer, dendrites and spines could be readily identified in the red channel (Supplementary Fig. S1B), and somata of GCs could be discerned up to 400 μm below the pial surface (Supplementary Fig. S1B; Supplementary Movie 1). Although only a few GC somata were labeled in the example in Supplementary Fig. S1B, GCs could be labeled at varying densities by titrating the amount of virus–for experiments on somatic imaging we used high titers for dense labeling. Odors were delivered using a custom-built olfactometer and GCs were imaged at a sampling rate of 4–8 Hz (see Methods). Odor stimulation caused an increase in fluorescence in GC somata (Supplementary Movie 2), with the number of responding cells varying with odor identity (Fig. 1A). In addition to discrete somatic regions, neuropil responses could often be observed, presumably due to dendrites of GCs located in deeper layers.

Somatic regions were chosen for analysis based on the bright fluorescence in the red channel, and fluorescence changes in the GCaMP channel monitored (Fig. 1B). In most experiments, each stimulus was given only once since we had to strike a balance between the number of repeats and the number of cell-odor pairs we could obtain from a single experiment. Since we allowed a 60 s inter-trial interval to evacuate odors and to minimize effects of habituation, each series took 25 minutes to complete (20 odors times 15 + 60 seconds). In preliminary experiments, we performed repeats of a smaller number of odors and found that responses in individual GCs were reliable (Fig. 1C), as judged by the pairwise correlation across repeated presentations of the same odor (Supplementary Fig. S2A). Responses in different GC somata had differing amplitude and time course (Fig. 1B), which were dependent on the odorant. For each odorant, we ordered the responses by the average amplitude to visualize the extent of activation more clearly (Fig. 1B, right panels). This method of visualization demonstrates the diversity of temporal dynamics, which does not just depend on the response amplitude. For example, responses that are sustained beyond the odor presentation occur for different amplitudes. We use this mode of representation in subsequent figures for visual clarity.

Characterizing odor-evoked responses. We used a suite of 20 odorants to examine the responses of the GC population. The odorants were chosen to activate the dorsal surface of the mouse OB at differing densities (see below). A matrix of average response amplitudes from one experiment illustrates that some odors activated many GCs in the imaged region, while other odors activating hardly any cells (Fig. 1D). Visualizing only responses that were above a hard threshold value (0.05 in this example) makes the odor-dependent differences in the number of responding GCs clearer (Fig. 1D, bottom).

While stronger responses could clearly be distinguished from noise, weaker responses were harder to discern. To obtain an objective measure of the distribution of responses, we plotted the histogram of responses of all GC-odor pairs in a given experiment. We used the baseline fluorescence period to obtain a noise distribution for the $\Delta F/F$ measurements and fitted a normal distribution to it (Fig. 1E, red line). Deviations from this normal distribution are due to odor-evoked responses (Fig. 1E, green line in the inset). The signal and noise distributions are highly overlapping, and a significant portion of responses will be lost using a hard threshold (for example, 2 SD of the noise distribution). Although this cannot be avoided for identifying individual responses, we can estimate the total number of responses for each stimulus by subtracting out the noise distribution. Such a population analysis indicated that the fraction of GCs in the imaged region that are activated varies widely for different odors (Fig. 1F).

We performed several control experiments to rule out some biases in our recordings. First, we found the responses of individual GCs across multiple trials to be reliable (Fig. 1C, Supplementary Fig. S2A). Second, we found no systematic relation between the resting fluorescence of a GC and the maximal $\Delta F/F$ (Supplementary Fig. S2B), ruling out a dominant effect of expression level of GCaMP3 on responses. Third, we found that most of the imaged GCs are capable of responding to stimuli once GABAergic inhibition is attenuated pharmacologically (Supplementary Fig. S2C,D, Supplementary Movie 3), indicating that the lack of activity in a majority of GCs is due to insufficient synaptic drive. Finally, we also performed additional experiments with a newer generation indicator GCaMP5 (Supplementary Fig. S3), as well as other experiments in awake animals (Supplementary Fig. S4) which confirmed the basic conclusions of the study.

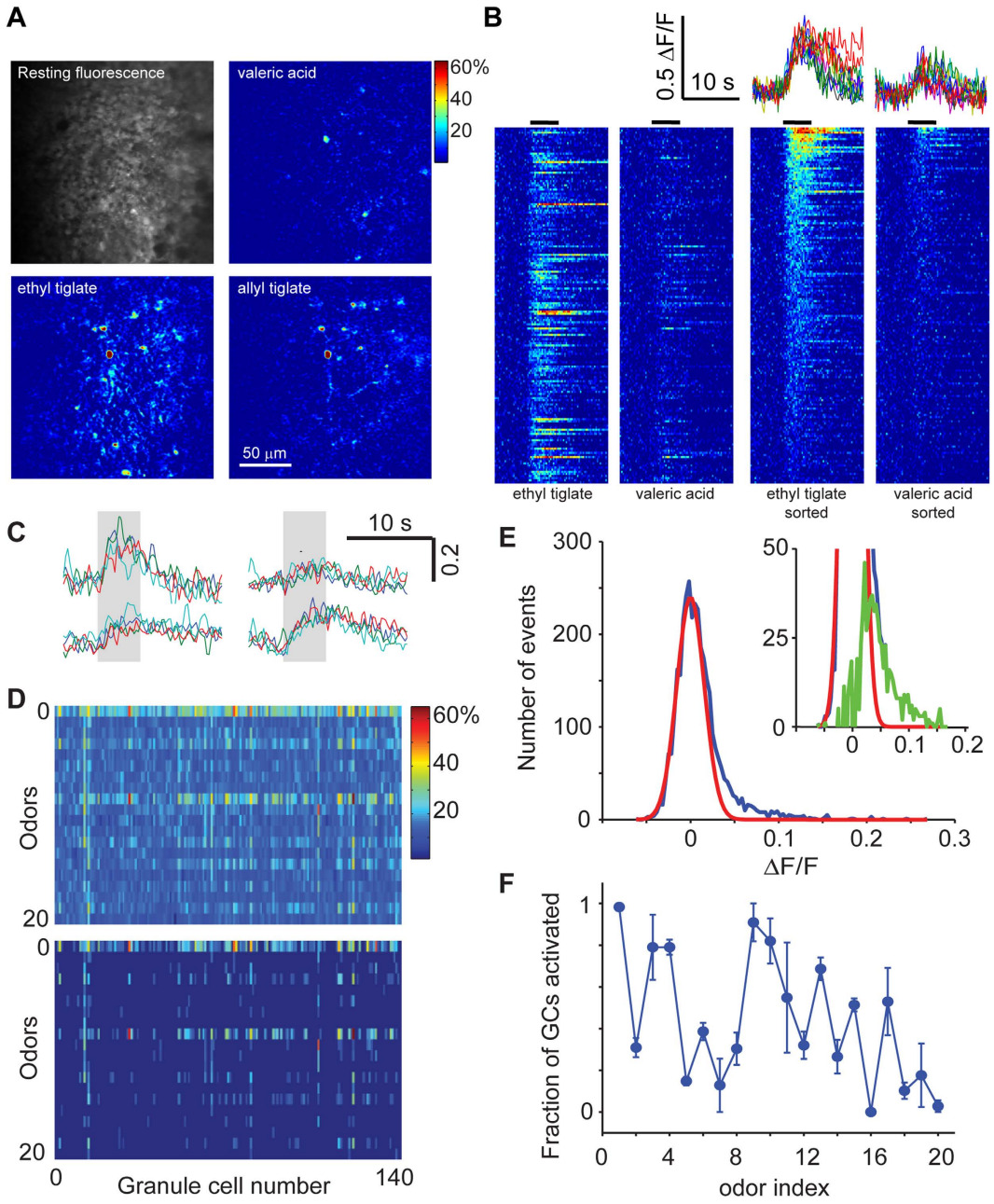

Figure 1. Characterizing odor responses in GCs. (**A**) Odor-evoked responses in cell bodies shown as differential fluorescence images. (**B**) Odor-evoked responses to 2 odors in 169 cells from a typical experiment. For each odor, responses are shown in arbitrary order in the left panels and in descending order of response amplitudes on right. Traces for 5 selected GCs are shown top right for 2 odors. Odor stimulus duration indicated by black lines above colormap panels. (**C**) Responses of 4 GCs to four separate presentations of allyl tiglate, illustrating the reliability of amplitude and time course. Odor stimulus indicated by gray rectangles. (**D**) Matrix of average responses of the 169 GCs to 20 odors. Top panel shows all the average ΔF/F values and the bottom matrix shows only those responses that are above a threshold of 0.05. (**E**) Distribution of average ΔF/F values for 3380 GC-odor pairs from the same experiment as above (blue) and the noise distribution calculated from baseline measurements (red). Inset shows the same distributions on an expanded scale, with the signal distribution (green) calculated as the difference between the blue and red distributions. (**F**) The relative fraction of GCs in imaged regions that were activated by each of the 20 odors, normalized to that for odor 1. Error bars are standard deviations (536 cells from 4 animals).

Temporal structure of responses. Although electrophysiological recordings have excellent temporal resolution, they are technically challenging and offer sparse sampling. We leveraged the high numbers afforded by population imaging to provide a comprehensive view of GC dynamics.

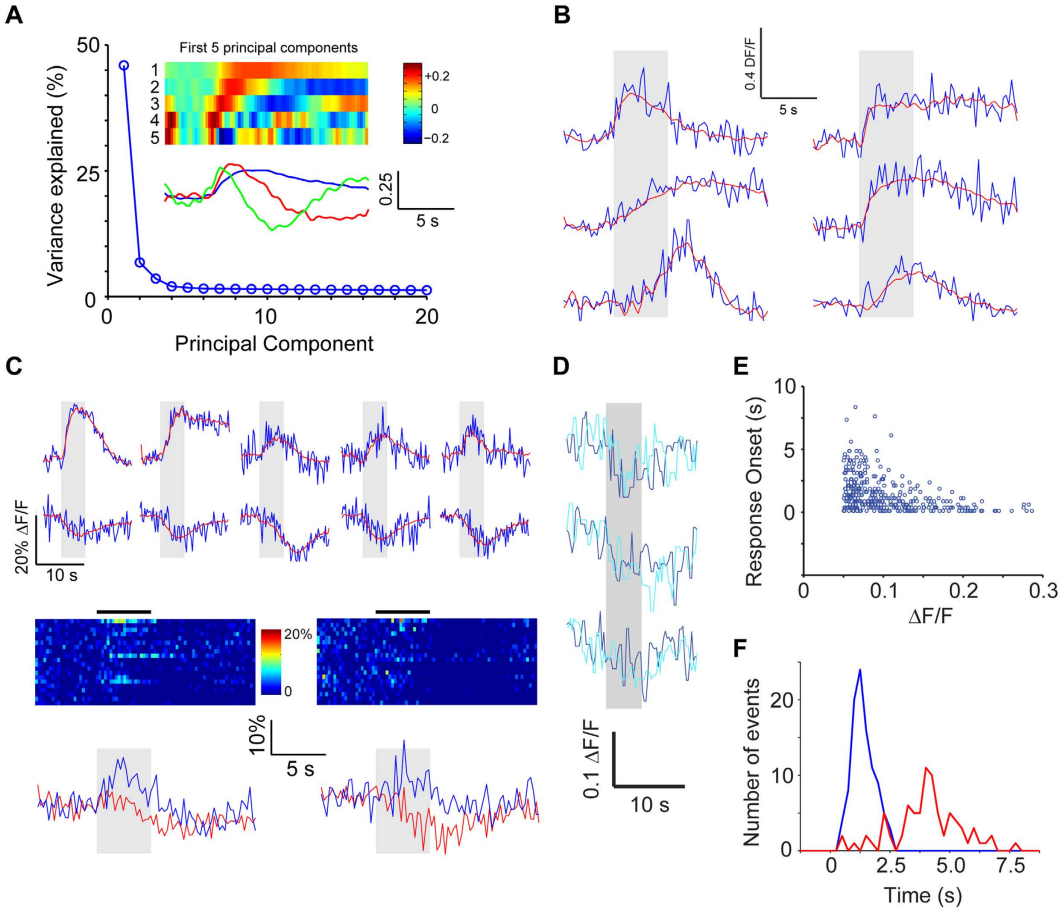

Figure 2. Temporal dynamics of GC responses. (**A**) PCA of the temporal profiles of responses of all GCs to all odors revealed that the first few principal components could explain most of the variance in the responses. The first 5 components are shown as color maps and only 3 components are shown as line traces below for clarity. 536 cells from 4 animals. (**B**) Examples of the time course of a few responses in GCs, with fits from the first 5 PCs (red) superimposed on raw fluorescence traces (blue). (**C**) Examples of inhibitory responses, along with additional examples of excitatory responses in the same experiment. Inhibitory responses could be well-explained by the same 5 PCs used for excitatory responses. The responses of two exemplar GCs to all 20 odors reveal that the same GC can have both excitatory and inhibitory responses to different odors. Selected traces are shown below for clarity. (**D**) Three examples of GCs with inhibitory responses across two trials. (**E**) Response latency (see Methods for details) for excitatory responses plotted against the average response amplitude (top) shows that strong responses had less variable, short latencies. (**F**) The distribution of response latency for inhibitory responses (red) was significantly ($p < 0.05$) shifted to the right compared to excitatory responses (blue).

The example recordings shown above (Fig. 1) hint at the diversity in the dynamics of odor responses. These included transient, accumulating, steady and delayed responses. To obtain an unbiased measure of the types of different temporal dynamics, we performed principal component analysis (PCA) of all responses (all GC-odor pairs) within a given experiment. We found that the first few principal components explained a large fraction of the variance in the time course of responses (Fig. 2A; 536 cells from 4 animals). A diversity of responses could be described well using 5 PCs (Fig. 2B). In addition to increases in fluorescence intensity upon odor stimulation, we also noticed reductions in fluorescence in some cases (Fig. 2C). These responses were defined as reductions in fluorescence that were greater than 5% of baseline fluctuation (see Methods), and were reliable across multiple trials (Fig. 2D). The response dynamics of a given neuron to different odors could be very different, with both inhibitory and excitatory responses (Fig. 2C, bottom). Inhibitory responses were far less frequent than excitatory responses (1061/8000 cell-odor pairs or 0.133 ± 0.008 excitatory responses vs. 83/8000 cell-odor pairs or 0.010 ± 0.002 inhibitory responses; $p < 0.001$), but the proportion of inhibitory responses will be an underestimate because of the low sensitivity of calcium imaging to hyperpolarization. The GABAergic antagonist bicuculline applied to the surface of the OB (see Methods) greatly reduced the fraction of GC responses that showed odor-evoked reductions (9/2888 or 0.003 ± 0.001 of cell-odor pairs, 160 cells from 2 animals, $p < 0.001$, Fisher's exact test, compared to the fraction without bicuculline above), indicating that the inhibitory responses are largely due to ionotropic GABAergic mechanisms.

We noticed that several odor responses occurred with significant delays following odor presentation (Fig. 2B). These delays were not due to stimulus dynamics because for the same stimulus, different GCs in the same imaged area could respond with different delays. When the delay was plotted as a function of response amplitude, it became clear that delayed responses were much more prevalent when the magnitude of the response was smaller (Fig. 2E). Such a relation could arise from the difficulty in detecting responses when the amplitude is small due to poorer signal-to-noise ratio. Alternately, there could be a threshold effect whereby smaller amplitude responses are typically a result of slow accumulation of synaptic input. Our data rule out the possibility that strong synchronous inputs arrive in a delayed manner after a period of quiescence. Instead, it would seem that if a GC receives strong excitation, it does so early on. We also found that inhibitory responses occurred, on average, with a greater delay than excitatory responses (Fig. 2F). The average delays for the strongest 100 positive and 80 negative responses (from the entire population of 536 cells from 4 animals) were 1.38 ± 0.48 and 4.03 ± 1.43 seconds respectively ($p < 0.001$; t-test).

Our data indicate that odor responses in GCs are heterogeneous and can be explained by a small number of elementary components. Interestingly, our imaging method is sensitive enough to detect inhibitory responses, which typically arise at longer delays following stimulation.

Density of GC activation depends on stimulus density. Different odorants activate differing number of GCs (Fig. 1). We wondered if there was a relation between the density of GC activation and the degree of activation of inputs to the OB. We first characterized the spatial extent of glomerular activation by the panel of odorants used in this study using mice expressing GCaMP3 in OSNs[48,49].

We imaged the glomerular inputs in OMP-GCaMP3 mice and recorded responses over a large region of the dorsal surface. Robust odor-evoked responses were imaged in the glomerular layer of OMP-GCaMP3 mice to many of the odors (Fig. 3A). The time course of responses varied depending on the glomerular and odor identities (Fig. 3B). By identifying all glomeruli in the imaged region using the resting fluorescence of GCaMP3, we estimated the fraction of glomeruli activated by a given odor. Averaging across 9 regions of interest (total of 127 glomeruli) and 4 animals, we determined that odorants in our panel activated between 0 and 30% of glomeruli imaged on the dorsal surface (Fig. 3B,C).

We next asked whether the density of responses of GCs was related to the fraction of activated glomeruli. Such a relation is inevitable in a purely feed-forward network, but lateral interactions within the OB could lead to winner-take-all-like activation, where a similar number of GCs could be activated by different odorants[50]. We used two measures to represent the density of activity of GCs. First, we simply summed the responses of all labeled GCs to each odor, and plotted this summed activity against the fraction of glomeruli activated (Fig. 3D). The summed GC activity was strongly correlated with glomerular activation (correlation coefficient of 0.80 in example shown in Fig. 3D), with an average correlation coefficient of 0.80 ± 0.05 (SD, $N = 6$ animals, more than 50 GCs in each experiment). A similar strong correlation was also found when considering the fraction of active GCs in the imaged field of view (0.81 ± 0.04, $N = 6$ animals). These strong correlations were also present if we used a modified metric for glomerular activation that took into account the amplitude of glomerular responses, rather than treating them in an all-or-none manner.

A second measure of GC activation we used is the population sparseness, which is related to the fraction of GCs that are activated strongly by a given stimulus[51,52]. There are multiple ways of characterizing population sparseness[52], and we chose a metric that is designed for responses involving only positive values[51,52] (see Methods). We found that this measure was also highly correlated with the glomerular input activity (Supplementary Fig. S5), with an average correlation of 0.78 ± 0.04 ($N = 6$ animals). These data indicate strongly that the extent of activation of the GC population is determined in large part by the density of sensory input.

We next asked how responsive individual GCs are to odor stimuli. We arranged the odor tuning curve for each GC in a descending order of the response amplitude, and averaged these across all GCs (Fig. 3E; 690 GCs, 6 animals). Because of the strict rank ordering, the tail of this curve reflects a biased noise distribution, which can be estimated using Monte Carlo sampling from the measured noise distribution (see Methods). Comparing the data distribution with the null distribution revealed that on average a GC responded to 3 odors out of the 20 used (Fig. 3E). We also calculated a widely-used measure called lifetime sparseness[52], which does not rely on thresholds to define responses. This measure varied widely from cell to cell (Supplementary Fig. S5), but on average this measure confirmed the sparseness of GC responses noted above.

The measure of sparseness of GC responses is likely to be affected by the sensitivity of the reporter used. We performed additional experiments using a more sensitive indicator, GCaMP5 (Supplementary Fig. S3). Although more GCs were indeed activated by odors, the additional data confirmed the basic conclusion that the density of responses is strongly correlated with the extent of glomerular input (Supplementary Fig. S3).

These results indicate that the density of GC activation is related strongly to the extent of glomerular activation, and GCs can be readily recruited even in anesthetized animals through dense activation of glomeruli.

Concentration dependence of GC activity. We found that there was a strong correlation between the extent of glomerular activation and the density of active GCs. We wondered if this relation also applies to increasing concentration of a given odor, a more straightforward way of increasing stimulus strength than altering odor identity to activate more glomeruli (Fig. 4).

Our stimulus set included 4 concentrations of allyl tiglate, spanning 3 orders of magnitude as measured by a miniPID device. We first confirmed that glomerular input responses to these four concentrations were strictly monotonically increasing (Supplementary Fig. S6). We then sorted GC responses to the highest concentration of odorant and displayed the responses to other concentrations in the same order (Fig. 4A). Visually, it becomes clear that responses are stronger and more GCs are activated by increasing concentration. This can be quantified by taking the average fluorescence change across all GCs (Fig. 4B, upper left panel), revealing a monotonic

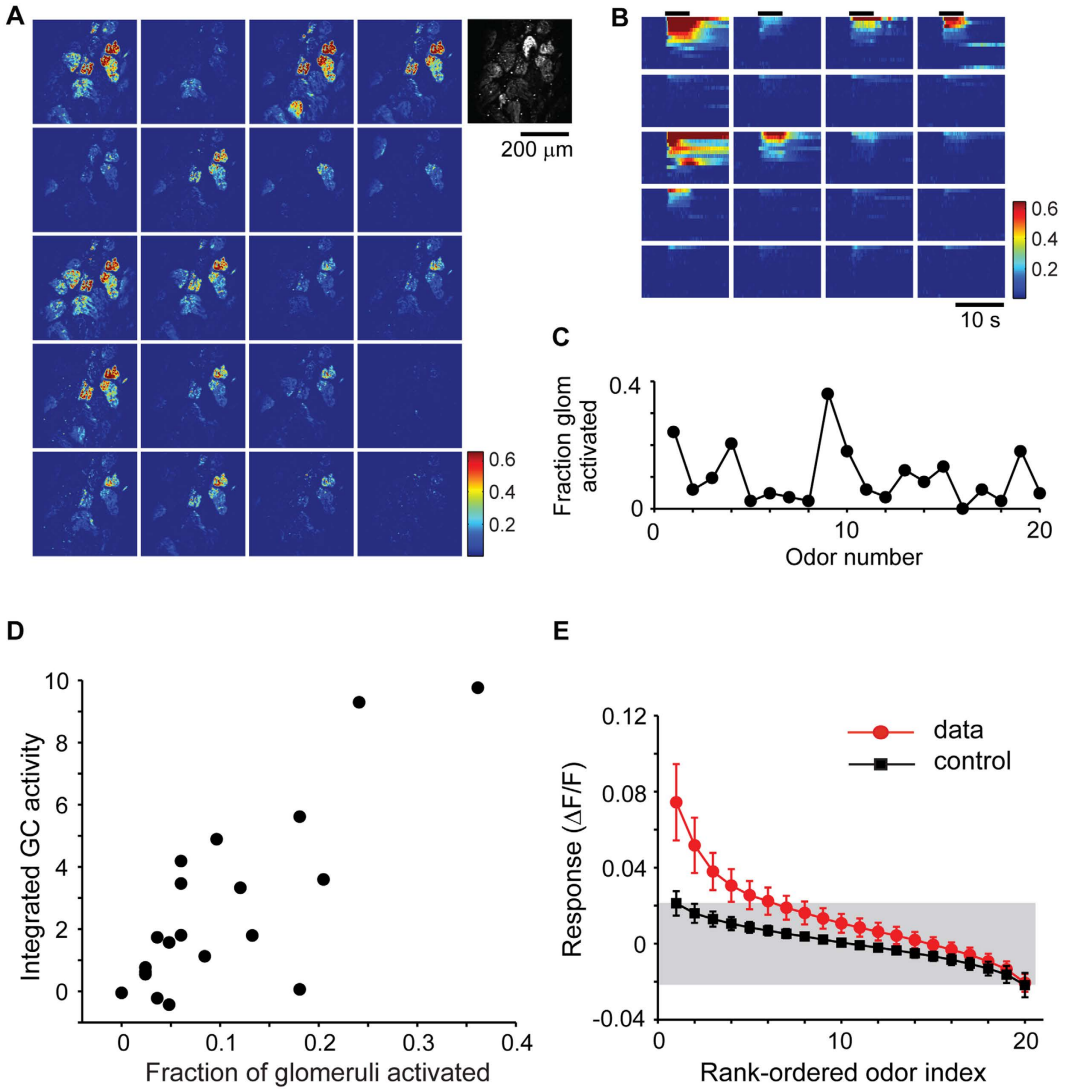

Figure 3. Response sparseness correlates with glomerular activation pattern. (**A**) The extent of glomerular activation by 20 odors was estimated by imaging responses in OMP-GCaMP3 mice. Fractional fluorescence changes for each of the odors are shown for one experiment, with the resting fluorescence shown at right in grayscale. (**B**) Time course of responses of individual glomeruli to all 20 odors (top). (**C**) Fraction of glomeruli activated (see Methods) varies widely for different odors (127 glomeruli from 4 animals). (**D**) The integrated activity of a population of GCs for a given odor is highly correlated with the fraction of glomeruli activated by that odor (representative experiment, averages in text). (**E**) Rank-ordered odor responses of GCs reveal that only a few odorants activate any given cell strongly. For each GC, the absolute values of responses were ranked in descending order and then the average across all GCs was obtained. Only the first 3 rank-ordered responses are significantly ($p < 0.05$) different from control plots from simulated data derived from the experimentally-observed noise distribution.

relation. Individual GCs display a range of dependence on concentration (Fig. 4B). We wondered whether all GCs have monotonic relation to odor concentration. To examine this issue objectively, for each experiment, we pooled GCs at the extreme of responses to the strongest concentration: 5 GCs that had the strongest responses, 5 GCs with responses in the middle range and 5 GCs with the weakest responses (or the most inhibited ones to be precise). We then examined the dependence of concentration of the responses of these GCs. This analysis uncovered a clear non-monotonic relation in a subset of GCs (Fig. 4C; 15 GCs selected with the above criteria from a total of 390 GCs from 3 animals), with the middle concentration giving rise to larger responses than the lower or higher concentration.

Since glomerular activation, at least in our experiments, always increased monotonically or saturated with odorant concentration (Supplementary Fig. S6), we reasoned that non-monotonic changes in individual GC activation are likely to be due to circuit interactions in the OB. In particular, it is possible that increasing activation of more glomeruli with increasing concentration could lead to lateral interactions within the OB that involve inhibition. We examined the concentration-dependence of GC responses in experiments where bicuculline was

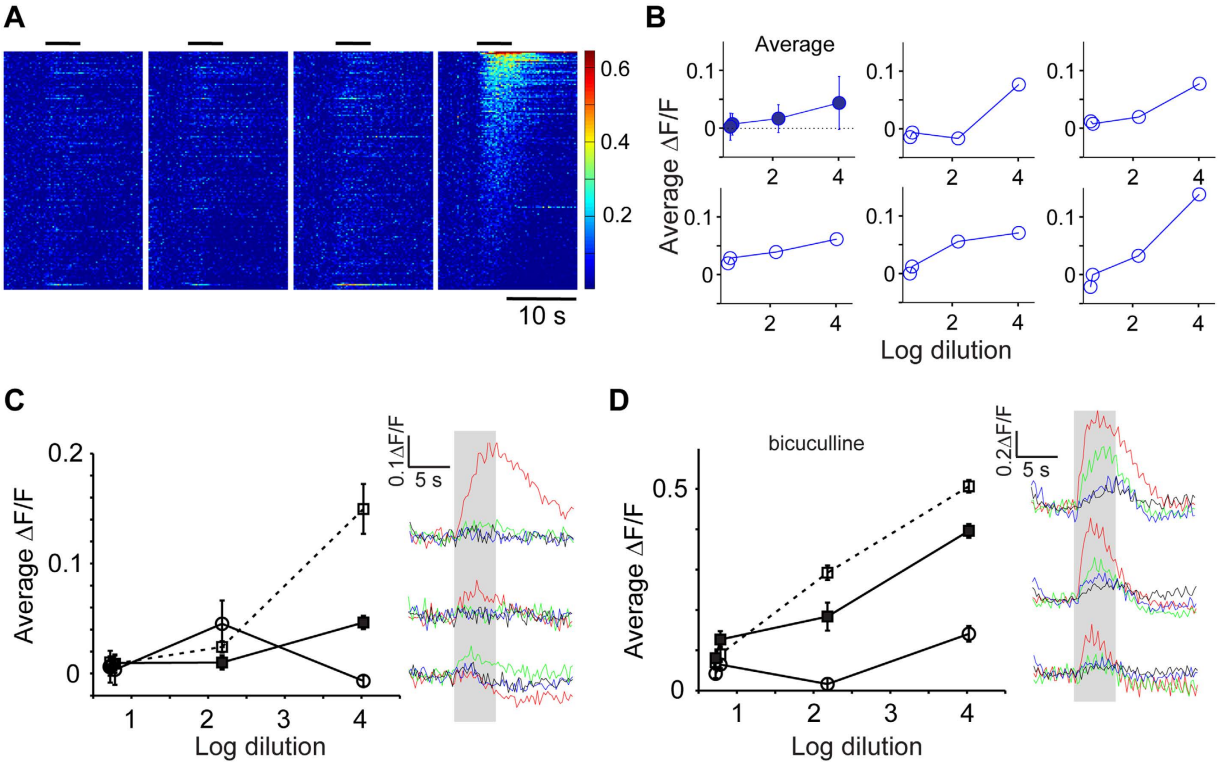

Figure 4. Effects of increasing concentration on GC responses. (**A**) Responses of all GCs from one experiment to four concentrations of allyl tiglate. Responses were arranged in descending order of amplitude for the highest concentrations and the rest of the plots followed the same GC rank order. (**B**) The average response to the four concentrations across the entire population (top left) and 5 randomly picked individual GCs. (**C**) Based on the highest concentration, 3 groups of 5 GCs were picked as the highest-amplitude responders, medium responders and the lowest amplitude responders. The responses of these three groups of GCs were then averaged for all concentrations, revealing non-monotonic responses as concentration increased. Time course of responses to the 4 concentrations are shown for the 3 groups at right (black, blue, green & red colors for increasing concentration). (**D**) A similar analysis in a different experiment performed after bicuculline was added to the surface of the OB showed no evidence of non-monotonic responses.

infused over the OB. We found that the non-monotonic relation observed for some GCs in control conditions was no longer found in experiments where inhibition was blocked with bicuculline (Fig. 4D; 2 animals).

Our data indicate that although many GCs are proportionally recruited by increasing stimulus intensity, other GCs can be inhibited at higher activation levels, leading to non-monotonic responses.

Spatial organization of responding GCs. We exploited our ability to record hundreds of GCs at once, to ask two questions about their spatial organization. First, are GCs that are close together functionally more similar than those located farther away? Second, are GCs responding to activation of a single glomerulus located in close proximity?

To answer the first question, we adapted an analysis method we developed previously[53]. In this method, we characterized the functional similarity of pairs of GCs by the cross correlation of their odor response spectra. GCs that respond in the same way to a panel of odors will have a correlation value close to 1, those that respond in an uncorrelated manner will have a value close to 0 and those that are anti-correlated will have a value of −1. We then plotted this similarity value for pairs of GCs as a function of their physical separation (Fig. 5A). Analysis over a large number of pairs (237,705 pairs, 6 animals) revealed no trend – that is, GC pairs separated by almost 300 microns were just as similar as those separated by a few microns (Fig. 5B). We compared this relation to a control one in which we preserved the distribution of spatial location of responding cells, but scrambled their response spectra. The observed relation was very similar to the control distribution, but had a slight dependence on distance (Fig. 5B).

Since neighboring glomeruli can be functionally quite dissimilar[53–55], any spatial clustering of responding GCs could be obscured by overlapping populations of GCs activated by neighboring glomeruli. We wondered if sparse activation of glomeruli may reveal clustered activation of GCs. Visual examination of the locations of active GCs suggested that odors with sparse glomerular activation (as characterized above in Fig. 3) activate a small number of GCs that appeared to be clustered within the imaged region (Fig. 5C). To quantify this impression, we calculated the average pair-wise separation between activated GCs for each odor and examined its relation to the sparseness of glomerular activation (Fig. 5D; 237,705 pairs, 6 animals in total). For odors that activated glomeruli sparsely, the average pairwise distance reached an asymptote of ~127 μm, which was the expected value

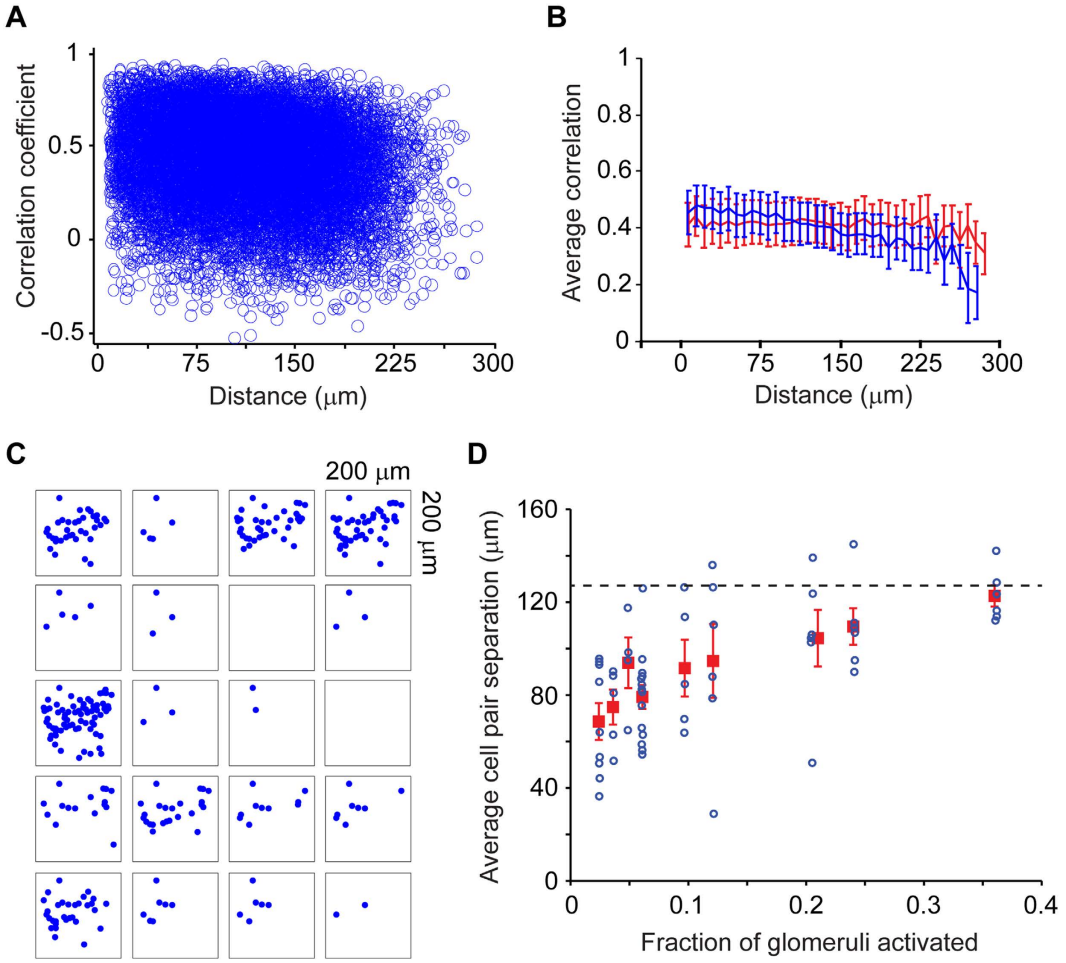

Figure 5. Spatial organization of responding GCs. **(A)** Scatter plot of similarity of GC odor tuning between a pair of GCs (calculated as cross correlation of their odor responses – see methods) and their spatial separation across all experiments. **(B)** The average similarity varies very little with separation, and is not significantly different from a control values calculated by randomizing odor response across GCs (red). **(C)** The spatial locations of active GCs for each of the odors in one experiment. Squares are 200 μm on the side. **(D)** The average pair-wise separation of GCs was calculated for each odor and plotted against the glomerular activation fraction for that odor. Blue circles are from individual experiments and averages are in red squares. Error bars are SEM. The dashed line is the expected average separation if GCs are activated randomly in terms of their spatial location. The trend for lower separations for sparsely-activating odors was significant ($p < 0.01$).

for random pairs of GCs selected from the imaged region (dashed line in Fig. 5D). Interestingly, the pairwise separation for GCs activated by "sparse" odors was smaller than those for denser odors ($p < 0.001$ with one-way ANOVA; $p < 2e^{-6}$ for a linear correlation analysis). This drop in pairwise separation was not an artifact of small numbers, since simulations of sparse random sampling from the population of imaged GCs led to higher variability in individual experiments, but not smaller separation (Supplementary Fig. S7).

These data suggest that GCs activated by a glomerulus in isolation are clustered, which could arise from either selective connectivity or from simple geometric considerations[5] (see Discussion).

Dendritic responses. Since GCs release neurotransmitter from their dendrites, their output can be modulated by local depolarization as well as cell-wide depolarization. Experiments in slices have indicated that both modes of depolarization can exist[17,21], but the occurrence of dendritic depolarization *in vivo* has remained in question. Imaging allowed us to examine directly how the apical dendrites of GCs respond to odorants.

We chose to first examine GC dendrites as a population by densely labeling GCs selectively using the VGAT-Cre mouse line[56]. By injecting virus to conditionally express GCaMP3 only in GABAergic interneurons, we ensured that there was no contribution of M/T cell dendrites when imaging was done in the EPL. Robust odor-evoked responses were observed in the EPL (Supplementary Fig. S8A,B). The amplitude of population responses in the EPL was strongly correlated with the density of glomerular activation (Supplementary Fig. S8C; correlation coefficient 0.79 ± 0.08; 3 animals), just as it was for GC somata. In one experiment, we examined responses in GC somata as well as in the EPL in the same preparation. The integrated activity was highly correlated in the two regions (Supplementary Fig. S8D).

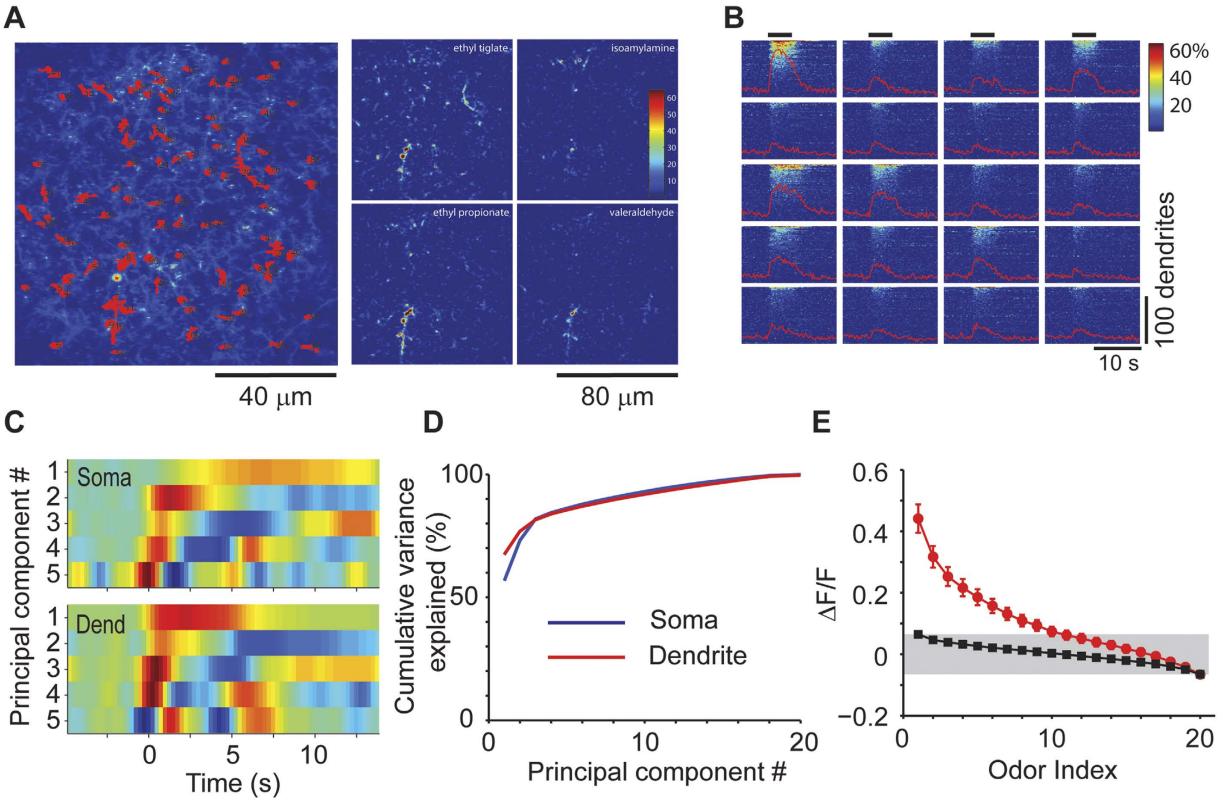

Figure 6. Responses in individual dendritic segments. (**A**) Sparse labeling of GCs using lentiviral injections into the OB allowed individual GC dendrites to be imaged (left) and their responses to odors measured (right). Only a fraction of the regions of interest are highlighted in red in the left image for clarity. (**B**) Time course of responses from 25 randomly chosen dendritic segments to 20 odors, arranged in descending order of response amplitudes for each odor. (**C**) PCA of time course of dendritic responses revealed faster dynamics of dendritic responses than those for somata (92 dendrites, 3 animals). (**D**) Most of the variance in time course of dendritic responses was accounted for by the first few components, as for GC somata (reproduced from Fig. 3A). (**E**) The average rank-ordered response amplitude distribution for dendrites revealed that they were generally more responsive than GC somata (92 dendrites, 3 animals ; compare Fig. 4E).

Examining average responses in the EPL is equivalent to recording local field potentials, and the dense labeling of many GCs did not allow us to resolve individual dendrites. To examine responses in individual dendritic segments of single GCs, we turned to sparse labeling using lentiviral infection (Fig. 6A). Imaging a region of interest that contained many dendrites, we could readily detect odor-evoked fluorescence increases (Fig. 6A,B; Supplementary Movie 4).

Individual dendritic elements respond to different subsets of odorants used; conversely some odorants evoked sparse responses and others denser activity (Fig. 6B). To examine the variation in temporal dynamics of responses, we performed principal component analysis in the same way as we did for somatic responses (Fig. 6C). We found that much of the variance of the data could be accounted for by the first few PCs (Fig. 6D; 92 dendrites, 3 animals). Although similar number of PCs were required to explain a given degree of variance for dendritic and somatic responses (Fig. 6D), the PCs had systematically faster time courses for dendrites than for GC somata (Fig. 6C).

We wondered whether dendrites would be more responsive than somata, since subthreshold synaptic activity could become visible in dendrites through local calcium rises. The number of odors activating a given piece of dendrite was indeed higher for dendrites, compared to somata (Fig. 6E; compare with Fig. 3E). Rank ordering odor responses for each dendrite and averaging across all dendrites revealed that a dendrite responded to 8 out of 20 odorants on average (92 dendrites, 3 animals), compared to 3 out of 20 for somata.

Local dendritic responses. We next sought to obtain direct evidence for dendritic responses that are independent of somatic responses. To this end, we labeled GCs sparsely using lentivirus injections and imaged the dendrites as well as cell body of visualized GCs (Fig. 7A). The soma and dendrites of the same neuron were identified by taking z-stacks of signals in the red channel. Comparing the responses of dendrites and soma revealed that many odors could activate both soma and dendrites (Fig. 7B). However, there were also dendritic responses to some odors, with no corresponding activation of somatic responses (*, Fig. 7B). This loss of response in the soma was not simply a result of different detection thresholds for dendrites and soma because a given level of dendritic response could either be accompanied by a somatic response (arrow, Fig. 7B) or not (*, Fig. 7B).

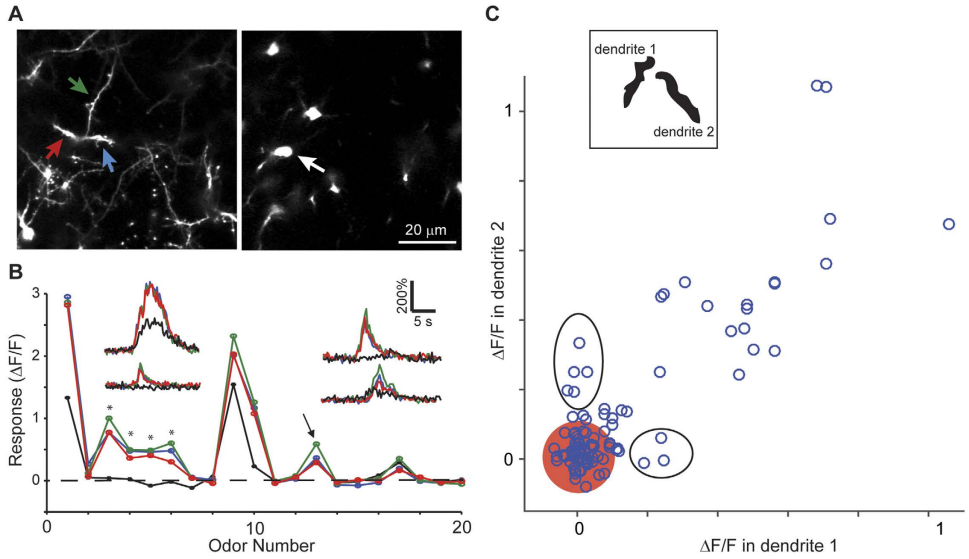

Figure 7. Dendritic responses can be local. **(A)** Dendrites and soma belonging to the same GC were identified through 3-dimensional reconstructions using the dTomato channel. **(B)** Average odor responses for all 20 odors in 3 dendritic segments and the corresponding soma. Dendritic responses to odors 3-6 were not accompanied by somatic responses (asterisks), but a similar magnitude response to odor 13 was accompanied by a somatic response. Insets show time course of odor responses of the 4 regions is shown for 4 selected odors. **(C)** Fluorescence change in pairs of dendrites of the same GC plotted against each other for all 20 odors. Red circle centered at the origin indicates 2 standard deviations of the noise, and ellipses highlight points representing selective dendritic responses that are well above noise.

Our scanning system did not allow us to scan at two different depths simultaneously, forcing us to image somatic and dendritic responses in different trials. Therefore, we focused our efforts on characterizing responses of multiple dendrites of the same GC imaged simultaneously. We looked for odor-evoked responses in an individual dendrite of a GC, in the absence of a response in a different dendrite of the same GC. We identified pairs of dendrites belonging to the same GC and displayed the response of one dendrite against a second dendrite for all 20 odors. Local and selective responses can then be discovered as outliers from the cloud of points along the diagonal (Fig. 7C). The experimental yield was lower since sparse labeling was necessary for these experiments (to trace dendrites from an identified GC). We found that 8 out of 34 events were local in the 5 pairs of dendrites we successfully identified that responded to at least one odor (Fig. 7C; 3 animals).

These data indicate that local dendritic responses can be occasionally recorded *in vivo*, demonstrating the possibility of independent dendritic processing.

Discussion

The function of GCs in the OB has been a matter of speculation for many decades. The biophysical properties of these cells and the reciprocal synapses with M/T cells have been studied in great detail[16,18–20,22,57], but their role in odor processing has been studied far less[13,36,37]. Here, we have shown that (i) the sparsity of GC population response has a strong relation to the extent of activation of glomerular inputs, (ii) activity of individual GCs can have complex, non-monotonic relationship to stimulus intensity, (iii) there is some degree of non-random spatial organization of GC responses, (iv) GC dendrites can respond independently to odors, potentially allowing local inhibition. Together, these findings suggest a specific role for GCs, distinct from general-purpose operations such as divisive normalization where participating interneurons indiscriminately integrate activity across many information channels.

Some caveats and justifications. Before discussing the implications of our study, it is important to acknowledge some caveats and rule out some concerns. First, like most other imaging methods, the signal-to-noise ratio does not approach spike recordings using electrodes, leading to an underestimation of neural activity. Our experiments were done with GCaMP3[47], because this was the best available sensor when the project was conceived and implemented. Although new sensors have better sensitivity[58], our main conclusions are still valid since all comparisons of importance were relative, and neither the absolute amplitude of responses nor the absolute number of responsive cells affect our conclusions. In addition, some of the key results were corroborated by experiments using a more sensitive indicator GCaMP5 (Supplementary Fig. S3).

A second, related concern is whether the expression level of the indicator biases responses in some way. This concern is significantly alleviated by our observation that there was no correlation between the resting fluorescence of GCs and the maximum response (Supplementary Fig. S2), which could have arisen from increased calcium buffering with increased expression levels[59,60]. We also found that a majority of cells in the imaged region are capable of responding to stimuli, as observed during application of bicuculline.

A third caveat is that we did not distinguish among potentially different classes of GCs–for example, in terms of depth of somata[61–63], neurochemical identity[64,65] or their age[63,66]. These will be the focus of future studies.

Fourth, the temporal resolution of signals (both due to the imaging speed and the time constants of the calcium indicator) limited our analysis to time scales of fraction of seconds, rather than milliseconds. Future experiments using speedier and more sensitive probes may allow us to extract faster modulation of activity, and examine its relation to breathing/sniffing.

Finally, there is a question whether imaging in anesthetized animals affects the conclusions made. Two recent studies have indicated that GCs become more responsive to odorants in awake animals[39,46]. We confirmed this finding in our preparation (Supplementary Fig. S4). In addition, we found that the increased responsiveness is due to larger responses in individual GCs in awake animals. Our data, combined with previous work, indicates that the overall pattern of activity in awake animals can be approximated by a scaled version of activity in anesthetized animals and therefore does not affect the basic conclusions in our study.

GC responses are diverse. The ability to record the activity of a large number of GCs allowed us to characterize their response features in a comprehensive manner. Electrophysiological recordings afford excellent signal-to-noise ratios, but have offered limited sample size because of technical challenges of recording from small neurons *in vivo*. They have, nevertheless, pointed to diverse temporal dynamics[42–45]. A previous imaging study also noted diverse temporal dynamics in responses, but focused on response onsets[39], which could be related to delayed activation seen in slice experiments[67]. Here, we performed principal component analysis of response dynamics and found that the diversity of temporal responses can be accounted for by a small number of primary shapes. In addition to previously reported temporal shapes of transient responses, we found evidence for accumulating or sustained responses (Fig. 2B). Temporal coding is thought to be prevalent in the vertebrate OB and its insect analog, arising through bulbar circuit dynamics[33,68–72]. Temporally diverse responses in GCs can sculpt mitral cell activity in complex ways, potentially increasing the coding capacity[73,74].

We also found evidence for inhibitory responses to odorants in GCs. Although many previous electrophysiological studies have not reported inhibitory responses to odorants in anesthetized animals, inhibitory currents could sometimes be recorded under voltage clamp[43,45]. This suggests that inhibitory currents were present, even when the overall responses were dominated by excitation. Inhibitory responses were abolished by blockade of $GABA_A$-mediated synaptic transmission. This finding, combined with the observation that inhibition typically appears later than excitation (Fig. 3E), indicates that intrabulbar circuit mechanisms underlie inhibitory responses. The source of functional inhibition is likely to be deep short axon cells[75,76], but other sources such as GCs themselves could also contribute. Finally, it is also possible that the fluorescence reduction could be due to reduction in tonic excitation provided by mitral and tufted cells.

Another novel finding of our study is that responses of GCs are not strictly monotonic as odorant concentration increases. Such non-monotonic responses were not observed in the presence of bicuculline, indicating that intrabulbar inhibition leads to this relation. Responses of principal cells to increasing concentrations have often been presented as being monotonic and saturating[44,77], but many other studies have found complex, non-monotonic dependencies of responses[78,79]. Non-monotonic responses in bulbar neurons (including GCs) may arise because additional, spatially disperse glomeruli will be recruited with increasing odorant concentration[80,81], leading to a shift in the balance of excitation and inhibition impinging on a given cell. For this reason, increasing concentration should not be seen as analogous to increasing stimulus intensities in other modalities, where the stimulus locus is held fixed.

GC response density scales with input. Another key finding of our study is that the response of GCs as a population scales well with the density of glomerular input. Electrophysiological recordings have hinted at weak responses to odorants in anesthetized rodent[42,43,46], but the sparseness of responses to a variety of odorants has not been studied systematically (but see ref. 44). Recent imaging studies have also noted that the responses of GCs are very sparse in anesthetized animals, again without characterizing the glomerular activation patterns of these odorants[39]. However, any discussion of the sparseness of responses of a population of neurons has to take into account the stimulus space. For example, in the visual system natural scenes lead to sparser encoding by cortical neurons than high contrast bars or gratings[82–84].

In this study, we examined the responses of GCs in relation to the inputs to the OB. We find that even in the anesthetized animal, the density GC responses as a population changes gradually with increasing number of activated glomeruli. Graded increase in the number of GCs could offer increasing inhibition to MCs as inputs become stronger, reducing saturation. It is, therefore, important to indicate how densely any particular odor stimuli activate glomeruli when quantifying response sparseness. In addition, our results also indicate that GCs are capable of responding to sensory inputs even when there is likely to be minimal feedback from higher brain areas, which is thought to be more prominent in the awake state[26,40,41,85].

Odor-evoked responses in GCs become denser in the awake compared to anesthetized state[39,46]. The reasons for this differential response sensitivity of GCs include state-dependent neuromodulation[86–89], differing extent of functional cortical feedback[26,28,40,85] and the presence of tonic inhibition[45]. We were able to confirm in our experiments that GCs are indeed more responsive to odor stimulation in the awake compared to anesthetized state (Supplementary Fig. S4). However, the basic conclusions of our studies in anesthetized animals are not affected since the relation between input structure and response density is preserved, and we found non-monotonic responses of some GCs to increasing odor concentration (Supplementary Fig. S4). In addition, we found that responses in awake animals are variable because of fluctuations in stimulus sampling due to sniff modulation, which made it harder to characterize response features from limited number of trials. We feel that responses in anesthetized animals are governed more by feedforward bulbar circuitry, establishing a ground state for further analysis in more awake and attentive states, where more complex higher order feedback will lead to variable

effects. Independent of the variation in the degree of sparseness in different brain states, our findings demonstrate that firing sparseness is related to the statistics of the sensory input itself.

Non-random spatial pattern of activation of GCs. Mitral cells with their primary dendrites in the same glomerulus are anatomically clustered in a small region, simply by geometric constraints[90]. Their lateral dendrites, however, span hundreds of microns and therefore become enmeshed with dendrites of mitral cells belonging to other glomeruli. Therefore, GCs activated by sister mitral cells can potentially be spatially distributed and intermingled with GCs activated by other dissimilar mitral cells[5]. Despite this distributed organization, there is anatomical evidence for potential clustering of GCs, but this is based on poorly understood trans-synaptic viral transport[91]. Experiments using c-fos labeling to quantify neural activation have also suggested clustered activation of GCs[92], but this method has unknown sensitivity. Using a real-time imaging method that has much better sensitivity and resolution, we found evidence for local functional clustering of GCs.

Initial analysis of the spatial pattern of activated GCs across all odorants revealed little order. However, any local order related to glomerular identity may be obscured because a single odorant can activate spatially distributed glomeruli and neighboring glomeruli can be functionally distinct[53–55]. We reasoned that odorants that activated glomeruli sparsely (ideally a single glomerulus) could reveal underlying spatial order of activated GCs. In line with this reasoning, we found that pairwise separation of active GCs was smaller for odors that activated glomeruli very sparsely, than for odors that had dense activation. This provides strong evidence that when a single glomerulus is stimulated, GCs that are activated are clustered spatially.

Does this clustering imply that there is selective synaptic connectivity, such that GCs in a small region get higher than chance inputs from sister mitral cells? Although we cannot rule out such selective functional synaptic connectivity, a simpler situation based on purely geometric considerations could allow clustered GC activation[5]. This is because, as sister mitral cells diverge, the chance that multiple lateral dendrites of sister MCs will activate neighboring GCs decreases as a square of the distance. Therefore, even with uniform connection probability along the lateral dendrite, a clustering of activated GCs will be observed. Future experiments combining functional and anatomical characterization will be necessary to disambiguate these possibilities.

It is not clear what such a clustering of GCs may accomplish. One possibility is that a cluster of functionally similar GCs can target the proximal dendrites of mitral/tufted cells within a local region to create a coarse and dynamic functional cell assembly[93].

Local dendritic processing. It has long been realized that the reciprocal synapses between M/T cells and GCs offer substrates for localized function[6,17,93]. Unlike axon-dendritic synapses, which generally rely on action potential propagation, local dendrodendritic synapses in the OB and other brain circuits such as the retina, can react to local depolarizations[94]. *In vitro* slice work has provided strong evidence that the dendrites of GCs can sustain local depolarization as well as global activity, presumably due to action potentials invading the entire dendritic tree[17,22]. Clear evidence for local dendritic calcium events and accompanying dendritic spike events recorded in the soma was also presented in the more intact frog nose-brain preparation[23]. Whether such local depolarizations occur *in vivo* in response to odor stimuli has remained unknown. Here, we offer strong evidence for the existence of local depolarization in GC dendrites *in vivo*.

First, we found that the average odor tuning curves for dendrites were broader than those for GC somata. This difference is unlikely to be simply due to differences in calcium buffering, since a careful study in slices has revealed no significant heterogeneity of calcium handling in GCs[95]. Second, the temporal dynamics of responses in dendrites were, at a population level, different from those in somata. Third and most directly, some odors could evoke calcium rises in dendrites without any detectable responses in the corresponding GC soma. This was not simply due to reduced sensitivity in the soma because other odors triggering fluorescence increases of similar magnitude in the dendrites can lead to detectable somatic signals as well.

What function could local dendritic activity in GCs have? Since many of the dendrodendritic synapses are reciprocal[6], local depolarization will mainly affect only those presynaptic mitral cells that caused the GC depolarization, leading to reciprocal or autoinhibition. By contrast, global depolarization of a GC can lead to lateral inhibition that affects other mitral/tufted cells.

GCs provide specific inhibition. It is now clear that interneurons in many regions of the brain are diverse[96,97], and each class of interneurons may have a specific functional role[97,98]. In the mouse retina, for example, there are more than 20 types of amacrine cells and their roles are beginning to be dissected[98]. In the OB, there is increasing evidence that some interneurons, including certain classes of glomerular-layer interneurons and parvalbumin-positive neurons in the external plexiform layer, may play a role in gain control or normalization[14,15]. Normalizing function has been well-studied in many regions of the brain and has attractive theoretical and conceptual implications[99,100]. However, for many circuit computations, more specific inhibition is necessary[2,98].

GCs in the OB have long been postulated to offer specific inhibition[16,50,101,102] and our study presents several experimental observations supporting this postulate. First, the existence of inhibitory responses in GCs is not readily predicted by models of global normalization. Second, non-monotonic responses in GCs with increasing concentration support a model of OB circuit function where there are competitive interactions among these cells, leading to dynamic and flexible inhibition of principal cells[9,50]. Again, this is in contrast to interneurons that function to integrate increasing inputs in a monotonic manner, and provide normalizing inhibition to principal cells[14,15]. Finally, the existence of local dendritic responses independent of the GC soma also strongly suggests that GCs can influence their targets more locally. Collectively, our data adds support to the idea that GCs mediate local and feature-specific inhibition. Such local dendritic responses in amacrine cells have been shown to be a key feature of direction selective responses in the retina[94,98]. In the OB, our data suggest that GCs do not simply

integrate the activity of all glomerular channels, but can selectively pool information from specific glomeruli. A careful consideration of odorant stimulus features and the glomeruli they activate may catalyze experiments illuminating GC function in the OB.

Materials and Methods

Animals and Surgery. Adult, 8 to 12 week-old male C57BL/6 (Charles River), VGAT-ires-Cre (Jackson Laboratory strain *Slc32a1*$^{tm2(cre)Lowl}$/J) or OMP-GCaMP3 mice (Isogai *et al.*) were anesthetized with an intraperitoneal injection of ketamine (90 mg/kg) and xylazine (10 mg/kg) and body temperature was maintained at 37 °C by a heating blanket (Harvard Apparatus). For viral injections a small craniotomy was made over the olfactory bulb and 100 nl of AAV2/9 or 300 nl of lentivirus was injected at a depth of 700 μm below the dural surface through a glass micropipette attached to a nanoinjector (MO-10, Narishige). To create an optical window an aluminum plate was glued to the skull, and the olfactory bulbs were exposed by making a craniotomy on either hemisphere using a dental drill. The surface was kept moist with artificial cerebrospinal fluid (aCSF; 125 mM NaCl, 5 mM KCl, 10 mM Glucose,10 mM HEPES, 2 mM CaCl2 and 2 mM MgSO4 [pH 7.4]). Before imaging, 1% agarose in aCSF was placed on the bulb and the window was closed with a coverslip. To block inhibition a small cut through the dura was made at the periphery of the craniotomy and a solution of 1% agarose in aCSF containing 100 μM (−)-Bicuculline methiodide (Tocris) was applied to the bulbar surface. All experiments were performed in accordance with the guidelines set by the National Institutes of Health and approved by the Institutional Animal Care and Use Committee at Harvard University.

Viral vectors. Granule cells were labeled with AAV2/9 expressing tdTomato and GCaMP3 under control of the CMV early enhancer/chicken β actin (CAG) promoter. Bicistronic expression was achieved by using a ribosomal skip site (T2A) between the two fluorophores. For conditional expression in VGAT-Cre mice we used AAV carrying floxed GCaMP3. AAV vectors were produced by the University of Pennsylvania Viral Vector Core. For sparse labeling we made use of a Tet-Off lentiviral system[103] with one construct expressing the transactivator tTAad under control of a synapsin promotor and a second construct expressing tdTomato-T2A-GCaMP3 under control of a TRE promoter. VSV-G pseudotyped lentiviral vectors were produced by transfection of human embryonic kidney cells (HEK293) with third-generation lentivirus plasmids using lipofection (Mirus). Supernatant was collected 48 h after transfection and concentrated using centrifugal filters (Millipore).

Immunohistochemistry. Three weeks after surgery, virus-injected mice were deeply anesthetized with a Ketamine (180 mg/kg i.p.)/Xylazine (20 mg/kg, i.p.) mixture and perfused transcardially with 20 ml of PBS (pH 7.4) first, followed by 50 ml of 4% paraformaldehyde in 0.1 M phosphate buffer (pH 7.4). Brains were removed and cut into 70 μm-thick sagittal sections with a vibratome (Leica). Sections were permeabilized and blocked with a solution containing 0.1% Triton X-100 (Tx, Fisher), 0.5% carrageenan (Sigma), and 2.5% goat serum in PBS for 1 h, and incubated overnight with primary antibody against GFP conjugated to Alexa 488 dye (Invitrogen) diluted 1:1000 in blocking solution. Sections were imaged with a confocal microscope (LSM 710, Zeiss).

***In vivo* imaging.** A custom-built two-photon microscope[104] was used for *in vivo* imaging. Fluorophores were excited and imaged with a water immersion objective (20×, 0.95 NA, Olympus) at 950 nm using a Ti:Sapphire laser (Mai Tai HP, Spectra-Physics). Frame rates were typically 4 Hz. Image acquisition and scanning were controlled by custom-written software in Labview. Emitted light was routed through two dichroic mirrors (680dcxr, Chroma and FF555-Di02, Semrock) and collected by 2 photomultiplier tubes (R3896, Hamamatsu) using filters in the 500–550 nm range (green channel, FF01-525/50, Semrock) and 572–642 nm range (red channel, FF01-607/70, Semrock).

To identify sparsely labeled granule cells that allow imaging of both their soma and dendrites the laser was tuned to 1020 nm and the red channel was used to record a detailed z-stack with 1 μm step size. The entire dendritic tree of a given GC was then examined to ensure that it could be clearly separated from processes of neighboring cells and faithfully traced to its corresponding soma. After choosing one imaging plane containing the soma and one imaging plane containing several branches of the same dendrite the laser was tuned back to 950 nm for imaging odor-evoked activity in either plane.

Odor stimulation. Following monomolecular odorants (Sigma) were used as stimuli and delivered by a custom-built 20 channel olfactometer controlled by custom-written software in Labview (National Instruments): ethyl tiglate (1), ethyl acrylate (2), valeric acid (3), allyl butyrate (4), isoamylamine (5), 2-methoxypyrazine (6), pyrrolidine (7), piperidine (8), allyl tiglate (9), valeraldehyde (10), isoamyl acetate (11), heptanal (12), iseugenol (13), ethyl propionate (14), 1-pentanol (15), 2-heptanone (16), p-anis aldehyde (17). Individual odors were presented for 5 s with an interstimulus interval of 60 s. Odorants were used at a nominal volumetric concentration of 1% (v/v) in mineral oil. For experiments testing the concentration dependence of responses, allyl tiglate was used at the following nomimal dilutions (v/v): 0.1%, 0.5%, 1% and 10%. The actual concentration ranges at the nose of the animal was estimated using measurements from a miniPID detector (Aurora). These values were then expressed as log dilution.

Data analysis. Data were analyzed offline using custom-written scripts in MATLAB (Mathworks). We selected regions of interest for analysis from averages of 100 or more individual images (to increase signal to noise ratio). Somata or dendritic segments were chosen based on fluorescence in the red (dTomato) channel. The average intensity in the green (GCaMP) channel was calculated for each ROI, for each frame and for each odor, leading to a 3D matrix of numbers.

A response value for each cell-odor pair was calculated as the average $\Delta F/F$ value over the 5 seconds of odor presentation. We performed receiver operating characteristic (ROC) analysis on our data and found a $\Delta F/F$ response threshold of 0.05-$\Delta F/F$ values above 0.05 were classified as excitatory responses and $\Delta F/F$ values below

−0.05 were classified as inhibitory responses. Since the noise distribution and signal distribution are highly overlapping (Fig. 2c), this threshold results in underestimating the number of responding cells. However, since most of the analysis relies on relative numbers, the exact number of responding cells will not affect our conclusions.

Temporal dynamics. Principal component analysis of the time course of responses was performed in Matlab (Mathworks) using centered data and singular value decomposition. The delay in the onset of responses was calculated from reconstruction of the time course using the first 5 principal components (which smoothed the data). Onset time was defined as the first time the ΔF/F value deviated from the baseline, if at least 3 subsequent points were 3 standard deviations above baseline fluctuation.

Rank ordered odor tuning. To facilitate averaging of odor tuning curves across all cells, we ordered individual tuning curves in descending order of amplitudes and averaged them across all cells. This average ordered tuning curve needs to be compared with a control tuning curve to estimate the number of odors an average GC responds to. The control curve was estimated as follows. We obtained a sample of 20 entries from a Gaussian noise distribution (Fig. 2c) and rank ordered them as if they were responses. We repeated this procedure 300 times to mimic many GCs, and averaged the rank-ordered tuning curves (obtained from a noise distribution). The maximum and minimum values of this null tuning curve gave us noise bounds, and the number of entries in the actual response tuning curve that exceeded these bounds gave us an estimate of the average number of odors that activated a GC.

Sparseness measures. To quantify the sparseness (or density) of activity of GCs, we estimated two measures: lifetime sparseness and population sparseness. Lifetime Sparseness quantifies the extent to which a given neuron is activated by different odor stimuli[52]. If all stimuli activate the observed element rather uniformly, the lifetime sparseness measure will be close to 1, and if only a small fraction of the stimuli activate the unit significantly, this metric will be close to 0.

$$LS_i = \frac{\left(\sum_{j=1}^{m} \frac{r_j}{m}\right)^2}{\sum_{j=1}^{m} \frac{r_j^2}{m}} \tag{1}$$

where m = *number of odors*, r_j = *response of neuron A to odor j.*

i refers to the index of the glomerulus A or cell body A, for which lifetime sparseness is calculated. Population Sparseness quantifies the fraction of elements (glomeruli or mitral cells) in the imaged field of view that respond to a given odor from the stimulus panel presented[52].

$$PS_j = \frac{\left(\sum_{i=1}^{n} \frac{r_i}{n}\right)^2}{\sum_{i=1}^{n} \frac{r_i^2}{n}} \tag{2}$$

where n = *number of neurons*, r_i = *response of neuron A to odor j.*

j refers to the index of the odor stimulus in the panel for which the population sparseness is calculated.

Response similarity and spatial separation. To quantify the similarity of response between pairs of GCs (indexed as A and B), we used the centered (Pearson) correlation coefficient:

$$C^{(A,B)} = \frac{\sum_{j=1}^{n}\left(r_j^A - \bar{r}^A\right)\left(r_j^B - \bar{r}^B\right)}{\sqrt{\sum_{j=1}^{n}\left(r_j^A - \bar{r}^A\right)^2}\sqrt{\sum_{j=1}^{n}\left(r_j^B - \bar{r}^B\right)^2}} \tag{3}$$

where

r_j^A = *response of neuron A to odor j*
$\bar{r}^A$ = *average response of neuron A to all odors*
r_j^B = *response of neuron B to odor j*
$\bar{r}^B$ = *average response of neuron B to all odors*
n = *number of odors*

We plotted the relationship between similarity and physical separation and averaged the similarity values by binning the data. Expected values for a random distribution were calculated by assigning randomly shuffled tuning curves to different GCs, and calculating pair-wise similarities.

Spatial distribution of responding GCs. The pair-wise separation of active GCs was calculated for each odorant, and the average separation for each odor was plotted against the extent of glomerular activation (Fig. 6D). The expected separation was estimated by sampling random pairs of GCs (from all the responding GCs within the imaged field of view). The effect of small sample numbers in potentially biasing the relation between glomerular sparseness and pairwise GC separation was assessed in the following way. We sampled randomly small number of GCs (equivalent to the numbers experimentally found for sparse odors) from the entire population of active GCs in a given experiment, and calculated the average pairwise separation. We repeated this sampling procedure multiple times to examine the scatter in the estimate of pairwise separation from small numbers of GC pairs. We found that the distribution of this average had high variance, but the average separation was close to the value predicted for all GCs (127 μm) (Supplementary Fig. S7).

References

1. Wilson, R. I. & Mainen, Z. F. Early events in olfactory processing. *Annu Rev Neurosci* **29,** 163–201 (2006).
2. Gollisch, T. & Meister, M. Eye Smarter than Scientists Believed: Neural Computations in Circuits of the Retina. *Neuron* **65,** 150–164 (2010).
3. Wilson, R. I. Early Olfactory Processing in *Drosophila* : Mechanisms and Principles. *Annual Review of Neuroscience* **36,** 217–241 (2013).
4. Mori, K. & Sakano, H. How is the olfactory map formed and interpreted in the mammalian brain? *Annu Rev Neurosci* **34,** 467–499 (2011).
5. Murthy, V. N. Olfactory maps in the brain. *Annu Rev Neurosci* **34,** 233–258 (2011).
6. Shepherd, G. M., Chen, W. R. & Greer, C. A. In *The synaptic organization of the brain* 165–216 (Oxford University Press, 2004).
7. Wachowiak, M. & Shipley, M. T. Coding and synaptic processing of sensory information in the glomerular layer of the olfactory bulb. *Semin Cell Dev Biol* **17,** 411–423 (2006).
8. Gire, D. H. & Schoppa, N. E. Control of on/off glomerular signaling by a local GABAergic microcircuit in the olfactory bulb. *J. Neurosci.* **29,** 13454–13464 (2009).
9. Cleland, T. A. Construction of odor representations by olfactory bulb microcircuits. *Prog. Brain Res.* **208,** 177–203 (2014).
10. Shao, Z., Puche, A. C., Liu, S. & Shipley, M. T. Intraglomerular inhibition shapes the strength and temporal structure of glomerular output. *J. Neurophysiol.* **108,** 782–793 (2012).
11. Olsen, S. R. & Wilson, R. I. Lateral presynaptic inhibition mediates gain control in an olfactory circuit. *Nature* **452,** 956–960 (2008).
12. Fukunaga, I., Berning, M., Kollo, M., Schmaltz, A. & Schaefer, A. T. Two distinct channels of olfactory bulb output. *Neuron* **75,** 320–329 (2012).
13. Fukunaga, I., Herb, J. T., Kollo, M., Boyden, E. S. & Schaefer, A. T. Independent control of gamma and theta activity by distinct interneuron networks in the olfactory bulb. *Nat. Neurosci.* **17,** 1208–1216 (2014).
14. Kato, H. K., Gillet, S. N., Peters, A. J., Isaacson, J. S. & Komiyama, T. Parvalbumin-expressing interneurons linearly control olfactory bulb output. *Neuron* **80,** 1218–1231 (2013).
15. Miyamichi, K. *et al.* Dissecting local circuits: parvalbumin interneurons underlie broad feedback control of olfactory bulb output. *Neuron* **80,** 1232–1245 (2013).
16. Shepherd, G. M., Chen, W. R., Willhite, D., Migliore, M. & Greer, C. A. The olfactory granule cell: from classical enigma to central role in olfactory processing. *Brain Res Rev* **55,** 373–382 (2007).
17. Egger, V., Svoboda, K. & Mainen, Z. F. Dendrodendritic synaptic signals in olfactory bulb granule cells: local spine boost and global low-threshold spike. *J. Neurosci.* **25,** 3521–3530 (2005).
18. Jahr, C. E. & Nicoll, R. A. Dendrodendritic inhibition: demonstration with intracellular recording. *Science* **207,** 1473–1475 (1980).
19. Isaacson, J. S. & Strowbridge, B. W. Olfactory reciprocal synapses: dendritic signaling in the CNS. *Neuron* **20,** 749–761 (1998).
20. Schoppa, N. E., Kinzie, J. M., Sahara, Y., Segerson, T. P. & Westbrook, G. L. Dendrodendritic inhibition in the olfactory bulb is driven by NMDA receptors. *J Neurosci* **18,** 6790–6802 (1998).
21. Bywalez, W. G. *et al.* Local postsynaptic voltage-gated sodium channel activation in dendritic spines of olfactory bulb granule cells. *Neuron* **85,** 590–601 (2015).
22. Egger, V., Svoboda, K. & Mainen, Z. F. Mechanisms of lateral inhibition in the olfactory bulb: efficiency and modulation of spike-evoked calcium influx into granule cells. *J. Neurosci.* **23,** 7551–7558 (2003).
23. Zelles, T., Boyd, J. D., Hardy, A. B. & Delaney, K. R. Branch-specific Ca2+ influx from Na+-dependent dendritic spikes in olfactory granule cells. *J. Neurosci.* **26,** 30–40 (2006).
24. Wiechert, M. T., Judkewitz, B., Riecke, H. & Friedrich, R. W. Mechanisms of pattern decorrelation by recurrent neuronal circuits. *Nat Neurosci* **13,** 1003–1010 (2010).
25. McTavish, T. S., Migliore, M., Shepherd, G. M. & Hines, M. L. Mitral cell spike synchrony modulated by dendrodendritic synapse location. *Front Comput Neurosci* **6,** 3 (2012).
26. Boyd, A. M., Sturgill, J. F., Poo, C. & Isaacson, J. S. Cortical feedback control of olfactory bulb circuits. *Neuron* **76,** 1161–1174 (2012).
27. Davis, B. J. & Macrides, F. The organization of centrifugal projections from the anterior olfactory nucleus, ventral hippocampal rudiment, and piriform cortex to the main olfactory bulb in the hamster: an autoradiographic study. *J Comp Neurol* **203,** 475–493 (1981).
28. Markopoulos, F., Rokni, D., Gire, D. H. & Murthy, V. N. Functional properties of cortical feedback projections to the olfactory bulb. *Neuron* **76,** 1175–1188 (2012).
29. Strowbridge, B. W. Role of cortical feedback in regulating inhibitory microcircuits. *Ann N Y Acad Sci.* **1170,** 270–274 (2009).
30. Balu, R., Larimer, P. & Strowbridge, B. W. Phasic stimuli evoke precisely timed spikes in intermittently discharging mitral cells. *J. Neurophysiol* **92,** 743–753 (2004).
31. Egger, V. & Urban, N. N. Dynamic connectivity in the mitral cell-granule cell microcircuit. *Semin Cell Dev Biol* **17,** 424–432 (2006).
32. Schoppa, N. E. Synchronization of olfactory bulb mitral cells by precisely timed inhibitory inputs. *Neuron* **49,** 271–283 (2006).
33. Dhawale, A. K., Hagiwara, A., Bhalla, U. S., Murthy, V. N. & Albeanu, D. F. Non-redundant odor coding by sister mitral cells revealed by light addressable glomeruli in the mouse. *Nat Neurosci* **13,** 1404–1412 (2010).
34. Arevian, A. C., Kapoor, V. & Urban, N. N. Activity-dependent gating of lateral inhibition in the mouse olfactory bulb. *Nat Neurosci* **11,** 80–87 (2008).
35. Lagier, S. *et al.* GABAergic inhibition at dendrodendritic synapses tunes gamma oscillations in the olfactory bulb. *Proc Natl Acad Sci USA* **104,** 7259–7264 (2007).
36. Abraham, N. M. *et al.* Synaptic Inhibition in the Olfactory Bulb Accelerates Odor Discrimination in Mice. *Neuron* **65,** 399–411 (2010).
37. Nunes, D. & Kuner, T. Disinhibition of olfactory bulb granule cells accelerates odour discrimination in mice. *Nat Commun* **6,** 8950 (2015).
38. Gilra, A. & Bhalla, U. S. Bulbar microcircuit model predicts connectivity and roles of interneurons in odor coding. *PLoS ONE* **10,** e0098045 (2015).
39. Kato, H. K., Chu, M. W., Isaacson, J. S. & Komiyama, T. Dynamic sensory representations in the olfactory bulb: modulation by wakefulness and experience. *Neuron* **76,** 962–975 (2012).
40. Otazu, G. H., Chae, H., Davis, M. B. & Albeanu, D. F. Cortical Feedback Decorrelates Olfactory Bulb Output in Awake Mice. *Neuron* **86,** 1461–1477 (2015).
41. Restrepo, D., Doucette, W., Whitesell, J. D., McTavish, T. S. & Salcedo, E. From the top down: flexible reading of a fragmented odor map. *Trends Neurosci* **32,** 525–531 (2009).
42. Wellis, D. P. & Scott, J. W. Intracellular responses of identified rat olfactory bulb interneurons to electrical and odor stimulation. *J. Neurophysiol* **64,** 932–947 (1990).
43. Cang, J. & Isaacson, J. S. *In vivo* whole-cell recording of odor-evoked synaptic transmission in the rat olfactory bulb. *J. Neurosci* **23,** 4108–4116 (2003).
44. Tan, J., Savigner, A., Ma, M. & Luo, M. Odor information processing by the olfactory bulb analyzed in gene-targeted mice. *Neuron* **65,** 912–926 (2010).

45. Labarrera, C., London, M. & Angelo, K. Tonic inhibition sets the state of excitability in olfactory bulb granule cells. *J. Physiol.* (*Lond.*) **591,** 1841–1850 (2013).
46. Cazakoff, B. N., Lau, B. Y. B., Crump, K. L., Demmer, H. S. & Shea, S. D. Broadly tuned and respiration-independent inhibition in the olfactory bulb of awake mice. *Nat. Neurosci.* doi: 10.1038/nn.3669 (2014).
47. Tian, L. *et al.* Imaging neural activity in worms, flies and mice with improved GCaMP calcium indicators. *Nat Methods* **6,** 875–881 (2009).
48. Isogai, Y. *et al.* Molecular organization of vomeronasal chemoreception. *Nature* **478,** 241–245 (2011).
49. Rokni, D., Hemmelder, V., Kapoor, V. & Murthy, V. N. An olfactory cocktail party: Fig.-ground segregation of odorants in rodents. *Nat. Neurosci.* **17,** 1225–1232 (2014).
50. Koulakov, A. A. & Rinberg, D. Sparse incomplete representations: a potential role of olfactory granule cells. *Neuron* **72,** 124–136 (2011).
51. Rolls, E. T. & Tovee, M. J. Sparseness of the neuronal representation of stimuli in the primate temporal visual cortex. *J. Neurophysiol.* **73,** 713–726 (1995).
52. Willmore, B. & Tolhurst, D. J. Characterizing the sparseness of neural codes. *Network* **12,** 255–270 (2001).
53. Soucy, E. R., Albeanu, D. F., Fantana, A. L., Murthy, V. N. & Meister, M. Precision and diversity in an odor map on the olfactory bulb. *Nat Neurosci* **12,** 210–220 (2009).
54. Bozza, T., McGann, J. P., Mombaerts, P. & Wachowiak, M. *In vivo* imaging of neuronal activity by targeted expression of a genetically encoded probe in the mouse. *Neuron* **42,** 9–21 (2004).
55. Ma, L. *et al.* Distributed representation of chemical features and tunotopic organization of glomeruli in the mouse olfactory bulb. *Proc. Natl. Acad. Sci. USA* **109,** 5481–5486 (2012).
56. Vong, L. *et al.* Leptin action on GABAergic neurons prevents obesity and reduces inhibitory tone to POMC neurons. *Neuron* **71,** 142–154 (2011).
57. Rall, W., Shepherd, G. M., Reese, T. S. & Brightman, M. W. Dendrodendritic synaptic pathway for inhibition in the olfactory bulb. *Exp. Neurol.* **14,** 44–56 (1966).
58. Chen, T.-W. *et al.* Ultrasensitive fluorescent proteins for imaging neuronal activity. *Nature* **499,** 295–300 (2013).
59. Helmchen, F., Imoto, K. & Sakmann, B. Ca2+ buffering and action potential-evoked Ca2+ signaling in dendrites of pyramidal neurons. *Biophys. J.* **70,** 1069–1081 (1996).
60. Maravall, M., Mainen, Z. F., Sabatini, B. L. & Svoboda, K. Estimating intracellular calcium concentrations and buffering without wavelength ratioing. *Biophys. J.* **78,** 2655–2667 (2000).
61. Mori, K., Kishi, K. & Ojima, H. Distribution of dendrites of mitral, displaced mitral, tufted, and granule cells in the rabbit olfactory bulb. *J Comp Neurol* **219,** 339–355 (1983).
62. Orona, E., Scott, J. W. & Rainer, E. C. Different granule cell populations innervate superficial and deep regions of the external plexiform layer in rat olfactory bulb. *J. Comp. Neurol.* **217,** 227–237 (1983).
63. Kelsch, W., Mosley, C. P., Lin, C.-W. & Lois, C. Distinct mammalian precursors are committed to generate neurons with defined dendritic projection patterns. *PLoS Biol.* **5,** e300 (2007).
64. Davis, B. J., Burd, G. D. & Macrides, F. Localization of methionine-enkephalin, substance P, and somatostatin immunoreactivities in the main olfactory bulb of the hamster. *J. Comp. Neurol.* **204,** 377–383 (1982).
65. Parrish-Aungst, S., Shipley, M. T., Erdelyi, F., Szabo, G. & Puche, A. C. Quantitative analysis of neuronal diversity in the mouse olfactory bulb. *J Comp Neurol* **501,** 825–836 (2007).
66. Lemasson, M., Saghatelyan, A., Olivo-Marin, J.-C. & Lledo, P.-M. Neonatal and adult neurogenesis provide two distinct populations of newborn neurons to the mouse olfactory bulb. *J. Neurosci.* **25,** 6816–6825 (2005).
67. Kapoor, V. & Urban, N. N. Glomerulus-specific, long-latency activity in the olfactory bulb granule cell network. *J Neurosci* **26,** 11709–11719 (2006).
68. Friedrich, R. W. & Stopfer, M. Recent dynamics in olfactory population coding. *Curr Opin Neurobiol* **11,** 468–474 (2001).
69. Laurent, G. Olfactory network dynamics and the coding of multidimensional signals. *Nat Rev Neurosci* **3,** 884–895 (2002).
70. Cury, K. M. & Uchida, N. Robust odor coding via inhalation-coupled transient activity in the mammalian olfactory bulb. *Neuron* **68,** 570–585 (2010).
71. Raman, B., Joseph, J., Tang, J. & Stopfer, M. Temporally diverse firing patterns in olfactory receptor neurons underlie spatiotemporal neural codes for odors. *J. Neurosci.* **30,** 1994–2006 (2010).
72. Shusterman, R., Smear, M. C., Koulakov, A. A. & Rinberg, D. Precise olfactory responses tile the sniff cycle. *Nat Neurosci* **14,** 1039–1044 (2011).
73. Giridhar, S. & Urban, N. N. Mechanisms and benefits of granule cell latency coding in the mouse olfactory bulb. *Front Neural Circuits* **6,** 40 (2012).
74. Tripathy, S. J., Padmanabhan, K., Gerkin, R. C. & Urban, N. N. Intermediate intrinsic diversity enhances neural population coding. *Proc. Natl. Acad. Sci. USA* **110,** 8248–8253 (2013).
75. Schneider, S. P. & Macrides, F. Laminar distributions of internuerons in the main olfactory bulb of the adult hamster. *Brain Res Bull* **3,** 73–82 (1978).
76. Arenkiel, B. R. *et al.* Activity-induced remodeling of olfactory bulb microcircuits revealed by monosynaptic tracing. *PLoS ONE* **6,** e29423 (2011).
77. Davison, I. G. & Katz, L. C. Sparse and selective odor coding by mitral/tufted neurons in the main olfactory bulb. *J Neurosci* **27,** 2091–2101 (2007).
78. Meredith, M. Patterned response to odor in mammalian olfactory bulb: the influence of intensity. *J Neurophysiol* **56,** 572–597 (1986).
79. Wellis, D. P., Scott, J. W. & Harrison, T. A. Discrimination among odorants by single neurons of the rat olfactory bulb. *J Neurophysiol* **61,** 1161–1177 (1989).
80. Rubin, B. D. & Katz, L. C. Optical imaging of odorant representations in the mammalian olfactory bulb. *Neuron* **23,** 499–511 (1999).
81. Meister, M. & Bonhoeffer, T. Tuning and topography in an odor map on the rat olfactory bulb. *J Neurosci* **21,** 1351–1360 (2001).
82. Vinje, W. E. & Gallant, J. L. Sparse coding and decorrelation in primary visual cortex during natural vision. *Science* **287,** 1273–1276 (2000).
83. Weliky, M., Fiser, J., Hunt, R. H. & Wagner, D. N. Coding of natural scenes in primary visual cortex. *Neuron* **37,** 703–718 (2003).
84. Froudarakis, E. *et al.* Population code in mouse V1 facilitates readout of natural scenes through increased sparseness. *Nat. Neurosci.* doi: 10.1038/nn.3707 (2014).
85. Boyd, A. M., Kato, H. K., Komiyama, T. & Isaacson, J. S. Broadcasting of Cortical Activity to the Olfactory Bulb. *Cell Reports* **10,** 1032–1039 (2015).
86. Kiselycznyk, C. L., Zhang, S. & Linster, C. Role of centrifugal projections to the olfactory bulb in olfactory processing. *Learn Mem* **13,** 575–579 (2006).
87. Petzold, G. C., Hagiwara, A. & Murthy, V. N. Serotonergic modulation of odor input to the mammalian olfactory bulb. *Nat. Neurosci.* **12,** 784–791 (2009).
88. Ma, M. & Luo, M. Optogenetic activation of basal forebrain cholinergic neurons modulates neuronal excitability and sensory responses in the main olfactory bulb. *J. Neurosci.* **32,** 10105–10116 (2012).

89. Rothermel, M., Carey, R. M., Puche, A., Shipley, M. T. & Wachowiak, M. Cholinergic inputs from Basal forebrain add an excitatory bias to odor coding in the olfactory bulb. *J. Neurosci.* **34,** 4654–4664 (2014).
90. Buonviso, N., Chaput, M. A. & Scott, J. W. Mitral cell-to-glomerulus connectivity: an HRP study of the orientation of mitral cell apical dendrites. *J Comp Neurol* **307,** 57–64 (1991).
91. Willhite, D. C. *et al.* Viral tracing identifies distributed columnar organization in the olfactory bulb. *Proc Natl Acad Sci USA* **103,** 12592–12597 (2006).
92. Guthrie, K. M., Anderson, A. J., Leon, M. & Gall, C. Odor-induced increases in c-fos mRNA expression reveal an anatomical 'unit' for odor processing in olfactory bulb. *Proc Natl Acad Sci USA* **90,** 3329–3333 (1993).
93. Yu, Y. *et al.* Sparse Distributed Representation of Odors in a Large-scale Olfactory Bulb Circuit. *PLoS Computational Biology* **9,** e1003014 (2013).
94. Euler, T., Detwiler, P. B. & Denk, W. Directionally selective calcium signals in dendrites of starburst amacrine cells. *Nature* **418,** 845–852 (2002).
95. Egger, V. & Stroh, O. Calcium buffering in rodent olfactory bulb granule cells and mitral cells. *J. Physiol.* (*Lond.*) **587,** 4467–4479 (2009).
96. Ascoli, G. A. *et al.* Petilla terminology: nomenclature of features of GABAergic interneurons of the cerebral cortex. *Nat. Rev. Neurosci.* **9,** 557–568 (2008).
97. Fishell, G. & Rudy, B. Mechanisms of inhibition within the telencephalon: 'where the wild things are'. *Annu. Rev. Neurosci.* **34,** 535–567 (2011).
98. Jadzinsky, P. D. & Baccus, S. A. Transformation of visual signals by inhibitory interneurons in retinal circuits. *Annu. Rev. Neurosci.* **36,** 403–428 (2013).
99. Isaacson, J. S. & Scanziani, M. How inhibition shapes cortical activity. *Neuron* **72,** 231–243 (2011).
100. Carandini, M. & Heeger, D. J. Normalization as a canonical neural computation. *Nat. Rev. Neurosci.* **13,** 51–62 (2012).
101. Cleland, T. A. Early transformations in odor representation. *Trends Neurosci* **33,** 130–139 (2010).
102. Wick, S. D., Wiechert, M. T., Friedrich, R. W. & Riecke, H. Pattern orthogonalization via channel decorrelation by adaptive networks. *J Comput Neurosci* **28,** 29–45 (2010).
103. Hioki, H. *et al.* High-level transgene expression in neurons by lentivirus with Tet-Off system. *Neurosci. Res.* **63,** 149–154 (2009).
104. Wienisch, M., Blauvelt, D. G., Sato, T. F. & Murthy, V. N. In *Neuronal Network Analysis* 67, 45–60 (Humana Press (Springer), 2012).

Acknowledgements

We thank the members of the Murthy Lab for fruitful discussions and comments on the manuscript. This research was supported by a HFSP Long-term fellowship to MW and funds from Harvard University and the NIH (DC11291).

Author Contributions

M.W. and V.N.M. designed the study, M.W. performed all experiments, M.W. and V.N.M. analyzed the data and wrote the paper.

Additional Information

Supplementary information accompanies this paper at http://www.nature.com/srep

Competing financial interests: The authors declare no competing financial interests.

How to cite this article: Wienisch, M. and Murthy, V. N. Population imaging at subcellular resolution supports specific and local inhibition by granule cells in the olfactory bulb. *Sci. Rep.* **6**, 29308; doi: 10.1038/srep29308 (2016).